Electron confinement in quantum nanostructures: Self-consistent Poisson-Schrödinger theory

James H. Luscombe and Ann M. Bouchard*
Central Research Laboratories, Texas Instruments, Inc., Dallas, Texas 75265

Marshall Luban
Ames Laboratory, Department of Physics and Astronomy, Iowa State University, Ames, Iowa 50011
(Received 26 June 1991; revised manuscript received 9 July 1992)

We compute the self-consistent electron states and confining potential, $V(r,T)$, for laterally confined cylindrical quantum wires at a temperature T from a numerical solution of the coupled Poisson and Schrödinger (PS) equations. Finite-temperature effects are included in the electron density function, $n(r,T)$, via the single-particle density matrix in the grand-canonical ensemble using the self-consistent bound states. We compare our results for a GaAs quantum wire with those obtained previously [J. H. Luscombe and M. Luban, Appl. Phys. Lett. **57**, 61 (1990)] from a finite-temperature Thomas-Fermi (TF) approximation. We find that the TF results agree well with those of the more realistic, but also more computationally intensive PS theory, except for low temperatures or for cases where the quantum wire is almost, but not totally, depleted due to a combination of either small geometry, surface boundary conditions, or low doping concentrations. In the latter situations, the number of subbands that are populated is relatively small, and both $n(r,T)$ and $V(r,T)$ exhibit Friedel-type oscillations. Otherwise the TF theory, which is based on free-particle states, is remarkably accurate. We also present results for the partial electron density functions associated with the angular momentum quantum numbers, and discuss their role in populating the quantum wire.

I. INTRODUCTION

In recent years there has been great progress in the ability to fabricate semiconductor structures with dimensions on the order of the electron wavelength.[1] Modern epitaxial techniques permit the control of atomic-scale features in the growth or vertical dimension, and nanolithography allows the patterning of structures with sub-100 nanometer (nm) lateral dimensions.[2,3] With suitable combinations of these characteristic length scales in the lateral and vertical directions, carrier confinement in up to all three spatial dimensions has been achieved in semiconductor nanostructures such that electron energy levels are quantized. It has been proposed that quantum nanostructures could form the basis for a future circuit technology, with the discrete energy levels ultimately determining device logic functions.[4,5] Examples include quantum wires, in which carriers are confined in two dimensions,[6] and quantum dots with three-dimensional electron confinement.[7,8] Whatever the confinement scheme, however, quantization is effected by an electron potential that depends, often sensitively, upon the details of the particular nanostructure embodiment. It is desirable, therefore, to have theoretical methods of calculating the electron potential that are applicable to a broad class of nanostructures.

The purpose of this paper is twofold. *First,* we compute the self-consistent electron density function $n(r,T)$ and confining potential $V(r,T)$ for laterally confined cylindrical quantum wires from a numerical solution of the coupled Poisson and Schrödinger (PS) equations. (Throughout this work, T denotes the temperature, we suppose that V is axially symmetric, and we employ the standard cylindrical coordinates r,θ,z.) We note that in nanostructures the requirement of self-consistency is of particular importance, since the carrier densities can vary substantially over the dimensions of the structure. Within the same structure in thermal equilibrium, electron densities can vary from highly degenerate in certain regions, to conditions of total depletion in others. Indeed, the unique transport properties of quantum devices hinge upon the creation of an inhomogeneous electron gas, where typically a depleted tunneling region separates neighboring electron populations in equilibrium with the Fermi levels established by the respective contacts. The role of the confining potential is thus twofold: V determines the electron states, while at the same time it is determined by the electrostatic action of the carriers in screening the fixed, neutralizing background charges (and by the boundary conditions imposed by the nanostructure). The *self-consistent* confining potential must be obtained, therefore, such that the electrons, in populating the quantum states associated with V, respond to the very same potential that they generate.

In previous work,[9] we have used a semi-classical Thomas-Fermi (TF) approximation, generalized to finite temperature, to compute the self-consistent screening potential of the inhomogeneous electron gas in quantum nanostructures. In that approach, $n(r,T)$ is taken to be the density of a free-electron gas in thermal equilibrium with the local value of the potential, so that

$$n_{\mathrm{TF}}(r,T)=\tfrac{1}{4}(2m^*/\pi\beta\hbar^2)^{3/2}F_{1/2}[\beta\{\mu-V(r,T)\}]\ . \quad (1)$$

In what follows, we suppress the temperature dependence of n and V. Here m^* is the effective mass, μ is the chemical potential (Fermi level), $\beta=1/(k_BT)$, and the function $F_{1/2}$ is a Fermi-Dirac integral[10] conventionally defined by

$$F_\alpha(\eta)=\frac{1}{\Gamma(\alpha+1)}\int_0^\infty dx\, x^\alpha[1+\exp(x-\eta)]^{-1} . \quad (2)$$

As shown in Refs. 5, 9, and 11, the TF model provides a robust theoretical framework in which one can readily compute the electron potential and carrier distribution in nanostructures with realistic epitaxial structures and boundary conditions. However, by treating the carriers as a free, three-dimensional Fermi gas, one thereby ignores the quantization of the electron states induced by the confining potential, which clearly raises the question of the method's applicability.

Thus, the *second* purpose of this paper is to contrast the results of the relatively simple TF approach with those of the coupled PS theory and thereby assess the validity of the TF approximation in laterally confined nanostructures. We find that in many cases the results of the TF approximation agree well with those of the more realistic, but also more computationally intensive PS theory. The situations where the results of the two theories do not agree are characterized by a relatively small number of populated subbands, either due to low temperature or to a condition of near depletion due to a combination of small lateral dimension, surface boundary conditions or low doping concentration. Otherwise, when more than several subbands are populated, the TF theory, which is based on free-particle states, is remarkably accurate and can serve as the basis for a fast-executing model of the confining potential in quantum nanostructures.

We consider the class of quantum wires that have an exposed lateral surface (at $r=R$). This is a relevant feature, since it establishes the boundary condition for $V(R)$, and, what is more important, the exposed surface provides the driving force for establishing the form of the confining potential. At the exposed surface of many semiconductors, the Fermi-level energy becomes "pinned" to a characteristic value in the band gap (independent of the dopant density), through a transfer of charge from interior energy levels to lower-energy, midgap surface states.[12] The Fermi-level pinning process thus depletes the surface region of carriers and is a primary mechanism for creating the inhomogeneous electron distributions mentioned above. We note that cylindrical quantum wires with exposed sidewalls are used to provide electrical contact with the resonant tunneling quantum dot studied in Ref. 7, where lateral confinement was achieved through a Fermi-level-pinning-induced depletion potential. Hence, the number of populated subbands is of relevance to the interpretation of quantum-dot transport studies.

A key issue for our cylindrically symmetric system is the role of the azimuthal angular momentum states in populating the quantum wire. Tunneling experiments on cylindrically symmetric quantum dots suggest that only zero angular momentum states contribute appreciably to the resonant tunneling current, due to the apparent insensitivity of the electrical transport characteristics to applied magnetic fields.[13] The notion of the quantum dot effectively filtering states of nonzero angular momentum from the resonant tunneling current has also been suggested theoretically from a consideration of the possible quantum-dot confining potentials consistent with the observed tunneling spectroscopy.[14] We find that the magnitude of the partial density functions associated with the nonzero angular momentum quantum numbers remains significant at a relatively large distance from the central axis of the quantum wire. Thus, these states would seemingly be available for resonant tunneling. More work, both theoretical and experimental, is required to better elucidate the transport characteristics of quantum dots.

In the next section, we formulate the basic equations governing the finite-temperature self-consistent potential and carrier density functions, and then outline the numerical methods by which convergence to a self-consistent solution is achieved. In Sec. III, we present our results and discuss the role of the angular momentum states, and compare these results with those of the TF treatment.

II. COUPLED POISSON-SCHRÖDINGER EQUATIONS

A. Self-consistent analysis

Achieving self-consistency involves solving two interconnected problems. The first consists of the quantum statistical mechanics problem of obtaining the electron density function from a given potential-energy function. The second involves the electrostatic problem of obtaining the potential generated by the charge distribution, from which the associated energy levels and states are derived.

We begin by obtaining, in the effective-mass approximation, the eigenstates of an electron that is bound in two dimensions by a cylindrically symmetric confining potential, $V(r)$, and which is free in the third dimension. Because of the axial and translational symmetries, the wave function factors in the usual way,

$$\psi_{l,m,k}=\frac{1}{\sqrt{L}}\Phi_{l,m}(r)e^{im\theta}e^{ikz} , \quad (3)$$

where $m=0,\pm1,\pm2,\ldots$ is the azimuthal quantum number, $l=1,2,3,\ldots$ is the radial quantum number, and L is the length of the cylinder. The subband spectrum is then labeled by three quantum numbers, $E_{l,m,k}=(\hbar^2/2m^*)k^2+\lambda_{l,m}$, where $\lambda_{l,m}$ is the eigenvalue associated with the eigenstate $\Phi_{l,m}$ of the radial Schrödinger equation,

$$\frac{-\hbar^2}{2m^*}\left[\frac{1}{r}\frac{d}{dr}\left[r\frac{d}{dr}\right]-\frac{m^2}{r^2}\right]\Phi_{l,m}(r)+V(r)\Phi_{l,m}(r)=\lambda_{l,m}\Phi_{l,m}(r) . \quad (4)$$

In the following, we assume that the $\Phi_{l,m}$ have been normalized according to

$$2\pi\int_0^R dr\, r\Phi_{l,m}^2(r)=1 . \quad (5)$$

Thus, the complete eigenfunction (3) is normalized to unity over the volume of the cylinder.

The radial eigenfunctions satisfy the following boundary conditions. At the exterior surface $\Phi_{l,m}(R)=0$, which corresponds to the requirement that the conduction electrons be confined to the volume of the quantum wire.[15] It can readily be shown from an analysis of the indicial equation for the solutions of (4) that at the origin, the states of nonzero angular momentum vanish, while the $m=0$ states have zero slope.

We obtain the finite-temperature electron density function from the thermal average of the single-particle density matrix in the grand-canonical ensemble.[16] Using the one-electron wave functions $\psi_{l,m,k}$, it can readily be shown that the density function is given by

$$n(r)=N_1\sum_{l,m}\Phi_{l,m}^2(r)F_{-1/2}[\beta(\mu-\lambda_{l,m})]\ , \tag{6}$$

where $N_1\equiv(2m^*/\pi\beta\hbar^2)^{1/2}$. Equation (6) gives the density of the electron gas at a distance r from the central axis. This expression can be interpreted as the summation of the product of the probability of finding the electron at point r in state $|l,m\rangle$, with the density of the one-dimensional electron gas that thermally populates the subband associated with energy $\lambda_{l,m}$.

Having derived an explicit expression for the electron density function, we then obtain the electrostatic potential ϕ from Poisson's equation,

$$-\frac{1}{r}\frac{d}{dr}\left[r\frac{d\phi(r)}{dr}\right]=\rho(\phi)\equiv\frac{e}{\epsilon}\{N_d-n[\phi(r)]\}\ , \tag{7}$$

where N_d is the number density of donors and where ϵ is the dielectric constant. We symbolically indicate that the charge density depends implicitly upon ϕ through the eigenvalues and eigenstates in (6). The potential energy V of the electron is given by $V=-e\phi$. For simplicity, we assume that the donors are uniformly distributed and remain ionized independent of the temperature. However, more complicated situations involving partially ionized donors or acceptor-hole distributions could also be investigated.

Equation (7) is to be solved subject to the Fermi-level-pinning boundary condition at $r=R$. We employ a commonly accepted value for the surface Fermi-level-pinning energy for GaAs of approximately half the band gap, $V(R)-\mu=0.7$ eV. Along the central axis, we demand that the radial electric field vanish, as required by the axial symmetry.

B. Numerical procedure

1. Schrödinger solution

Employing the standard three-point finite-difference approximation, the radial Schrödinger equation (4) is equivalent to the matrix eigenvalue problem $H\Phi=\lambda\Phi$, where H is tridiagonal. The form of H, however, is not symmetric (owing to the scale factors in the cylindrical Laplacian), and is also dependent on whether $m=0$ or not to incorporate the boundary conditions on $\Phi_{l,m}(0)$. We cast H into symmetric form with a similarity transformation[17] to take advantage of an efficient bisection search algorithm[18] that obtains the eigenvalues and eigenvectors of a real symmetric matrix within a given energy interval. It is the physical eigenvectors, however, that enter the calculation and must be normalized [Eq. (5)] at each iteration of the coupled PS computation. We search for all eigenvalues lying between the lowest value of the confining potential, and those within approximately $10k_BT$ above the Fermi-level energy. The Fermi-Dirac integral in (6) decreases exponentially for large negative argument, and thus it suffices to keep only a few eigenvalues above the Fermi level. We note that the number of radial eigenvalues below the Fermi level is dependent on the quantum number m. The larger the value of m, the fewer the number of electron states that are populated. This is because the eigenvalues associated with the *effective* potential (V combined with the quantum-mechanical centrifugal potential barrier) start well above the Fermi level for sufficiently high values of m. These issues are explored in greater detail below.

2. Self-consistent Poisson solution

We use a damped Newton method to solve the nonlinear Poisson equation (7). To optimize the procedure, we follow Laux and co-workers[19] in using the Bank-Rose parameter selection algorithm.[20] In this approach, starting from an initial guess for ϕ, one repeats solving the Schrödinger equation, computing $n(r)$, and then updating $\phi(r)$ via the Newton algorithm, until the iterates converge on the self-consistent solution. To initiate the procedure, we first compute the finite-temperature TF self-consistent potential, the differential equation for which results from using (1) in (7). The solution to this nonlinear differential equation subject to the Fermi-level-pinning boundary condition is discussed in Ref. 9.

As a check on the accuracy of the self-consistent solution, we monitor charge neutrality. From the Poisson equation, we readily derive the charge-balance equation:

$$N_1\sum_{l,m}F_{-1/2}[\beta(\mu-\lambda_{l,m})]+2\pi R\sigma=\pi R^2N_d\ , \tag{8}$$

where $\sigma\equiv(\epsilon/e^2)(dV/dr)_{r=R}$ and $-e\sigma$ is the charge on the exposed surface of the quantum wire per unit length. Recall that the existence of surface charge is associated with the Fermi-level-pinning boundary condition. Equation (8) expresses charge neutrality: Per unit length, the number of electrons populating subbands, plus the number occupying surface states equals the number of donor ions. Note that both quantities on the left-hand side of (8) are determined self-consistently, whereas the right-hand side is a fixed quantity. We find that (8) is typically obeyed to within one part in 10^6 by our self-consistent numerical solutions.

III. NUMERICAL RESULTS

The basic numerical results for this paper are summarized by Figs. 1–5. In Fig. 1(a) we show our results for the self-consistent PS confining potential and electron density function for a cylindrical GaAs quantum wire of

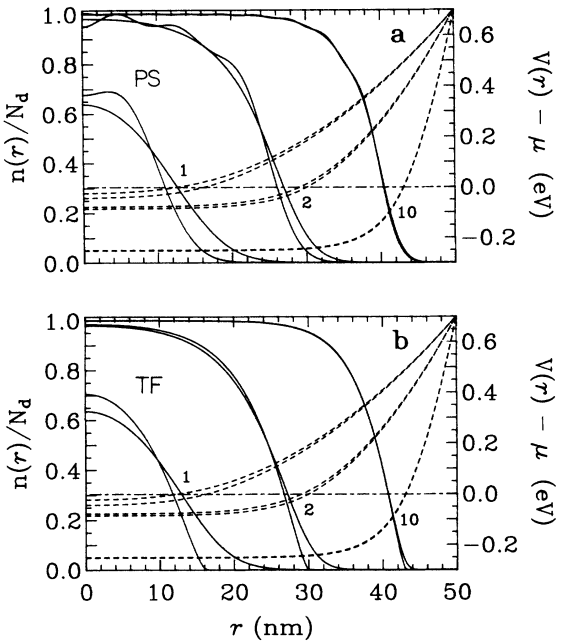

FIG. 1. Self-consistent confining potentials (dashed curves, right ordinate) and electron density functions (solid curves, left ordinate) for (a) Poisson-Schrödinger theory and (b) finite-temperature Thomas-Fermi approximation, for $T=10$ and 300 K and indicated doping densities (units of 10^{18} cm^{-3}).

50-nm radius with an exposed lateral surface, for several dopant concentrations (labeled in units of 10^{18} cm^{-3}) at temperatures $T=10$ and 300 K. The quantity $V(r)$ is shown as a dashed curve, and corresponds to the right ordinate. As remarked above, we have used the Fermi-level-pinning boundary condition $V(R)-\mu=0.7$ eV. The quantity $n(r)$ is shown as a solid curve corresponding to the left ordinate axis, and is given in units of N_d. Figure 1(b) shows the analogous quantities computed from a solution of the Poisson equation utilizing the TF expression for the electron density function, Eq. (1). Note the close resemblance of the TF results with those of the PS calculation. Below, we delve into the physics underlying the two sets of results in Figs. 1(a) and 1(b).

First, we observe some of the qualitative features common to the results of both calculations. Note that there is an appreciable electron population in the interior of the quantum wire wherever the confining potential is below the Fermi level, and that the electron density decays to zero as $V(r)$ crosses above the Fermi level. Moreover, the details of the decay are sensitive to the temperature. For the highest doping density shown, 10^{19} cm^{-3}, the results are essentially independent of the temperature. A useful temperature gauge is provided by the Fermi temperature of an electron gas with density equal to the dopant concentration, $k_B T_F \equiv \hbar^2(3\pi^2 N_d)^{2/3}/(2m^*)$. The Fermi temperature of an electron gas of density 10^{19} cm^{-3} in GaAs is approximately 2900 K. Thus, room temperature is ostensibly equivalent to zero temperature for this doping concentration, and accordingly, one cannot distinguish between results for the two temperatures in Fig. 1, except in the tail of the electron distribution as $n(r)$ vanishes. A decrease in the doping level to 10^{18} cm^{-3} is accompanied by a dramatic decrease in the electron density throughout the interior of the system, as well as increased sensitivity of the results to temperature. The Fermi temperatures associated with doping concentrations 2×10^{18} and 10^{18} are 1003 and 632 K, respectively. Note that for these cases, the structure is not just depleted near the outer surface; there is also a substantial reduction in electron density relative to the dopants at the center of the quantum wire. This partial depletion of the center of the structure becomes most sensitive to the details of the system when the value of $V(0)$ is closest to the Fermi level. Besides the temperature and doping level, the extent to which the structure is depleted depends on material parameters such as the effective mass and dielectric constant, as well as structural parameters such as the lateral dimension and the surface Fermi-level-pinning energy.

We have demonstrated previously for nanostructures with Fermi-level pinning that, within the TF approximation, at no point in the structure is there local charge balance, regardless of the doping density.[9] This can be proven analytically at zero temperature, and is found numerically at finite temperature.[9] Overall, of course, such systems are charge neutral; the seemingly missing electrons occupy the states at the surface that support Fermi-level pinning. Thus, the value of $n(0)/N_d$ in Fig. 1(b) for 10^{19} cm^{-3} is slightly less than unity. This deviation from charge neutrality at the center of the quantum wire is more dramatic the lower the value of N_d.

In Fig. 2, we show the behavior of $n(r)$ and $V(r)$ at low temperature in more detail, where a direct compar-

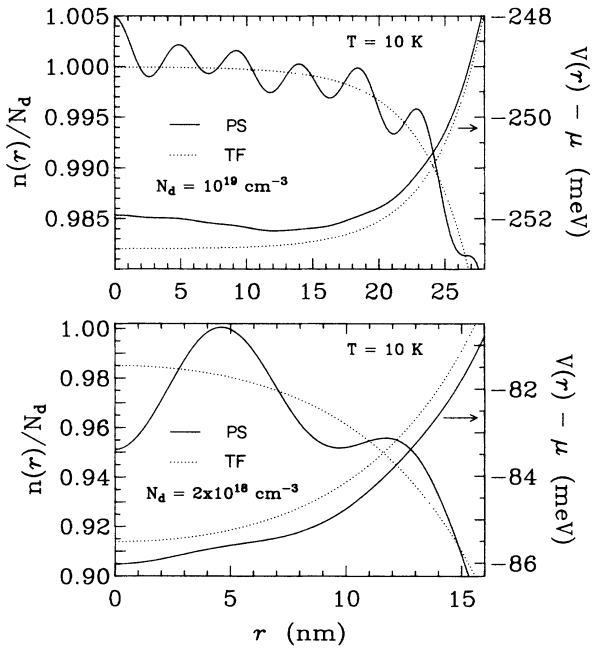

FIG. 2. Expanded view of self-consistent electron density functions (left ordinate) and confining potentials (right ordinate) for Poisson-Schrödinger calculation (solid curves) and Thomas-Fermi approximation (dotted curves) for two doping densities at $T=10$ K. Note Friedel-type spatial oscillations in the Poisson-Schrödinger results.

ison is made between the results of the PS and TF self-consistent theories. Here we see the qualitatively new features of the PS theory: first, the electron density function exhibits Friedel-type spatial oscillations,[21] and, second, in contrast to the TF results, the density of electrons can locally *exceed* that of the dopants. We note that the basic wavelength of the oscillations in Fig. 2 is approximately half the Fermi wavelength, which is consistent with the behavior of Friedel oscillations in bulk systems.[21] We also show a detailed comparison of the PS confining potential with the corresponding TF results. From Fig. 1, the potentials appear flat near the origin, and indeed the TF potentials can be extremely flat.[9] However, on the scale of Fig. 2, it is seen that the low-temperature PS potential also exhibits Friedel-type oscillations, which one would expect if the potential is self-consistent with an oscillatory charge-density function. One would also expect that a local excess of electrons over dopants would be accompanied by inflections in the self-consistent potential, due to the change in sign of the net charge density in Poisson's equation. This is confirmed in Fig. 2, where the curvature in $V(r)$ is locally negative wherever $n(r)$ exceeds N_d.

The physical origin of these oscillations can be traced to the behavior of the lateral bound-state eigenfunctions and the extent to which the associated subbands are populated. In Fig. 3, we show the partial electron density functions that result when the terms of the summation in (6) associated with a given value of $|m|$ are summed separately. Note that, as expected, the higher the value of $|m|$, the further out from the central axis are the partial electron densities peaked.

Figure 4 shows the bound-state eigenvalues $\lambda_{l,m}$ associated with the self-consistent potential for $N_d = 2\times10^{18}$ cm^{-3} as a function of the quantum number m. The dashed (dash-dot) line in the figure marks the energy $10k_BT$ above the Fermi level for $T=10$ K ($T=300$ K).

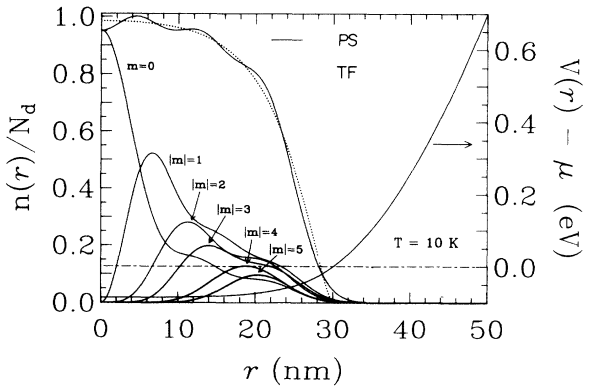

FIG. 3. Partial electron density functions at $T=10$ K associated with various values of the angular momentum quantum number, along with the total density function that results from summing the individual contributions for all values of $|m|$. Shown for comparison is the Thomas-Fermi self-consistent electron density function (dotted line), as well as the Poisson-Schrödinger confining potential, associated with the right ordinate. Results correspond to a quantum wire with doping level of 2×10^{18} cm^{-3}.

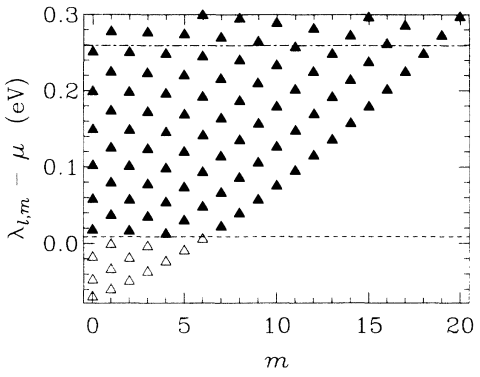

FIG. 4. Bound-state eigenvalues as a function of angular momentum quantum number for a doping level of 2×10^{18} cm^{-3}. Dashed (dash-dot) line is the energy $10k_BT$ above the Fermi level for $T=10$ K ($T=300$ K). Open triangles indicate the eigenvalues that make an appreciable contribution to the electron population at $T=10$ K, whereas at $T=300$ K both open and filled triangles contribute. The increased number of states that contributes to the electron population at the higher temperature leads to good agreement between the results of the PS and TF calculations (compare Figs. 3 and 5).

As a figure of merit, eigenvalues $10k_BT$ above the Fermi level make a negligible, exponentially small contribution to the electron population. Thus, for $T=10$ K, only the eigenvalues indicated with the open triangles contribute appreciably to the electron density,[22] whereas for $T=300$ K both open and filled triangles contribute. Note that the higher the value of m, the fewer the number of radial states that are populated. This is because the quantum-mechanical centrifugal energy barrier, for sufficiently large m, raises the effective confining potential such that, for a given temperature, even the lowest-energy states are negligibly populated. At $T=0$, only those states with eigenvalues below the Fermi level are occupied, and hence the summation of the squared eigenfunctions for these few modes produces Friedel oscillations. For low temperatures, or for cases when the structure is substantially depleted, there are also sufficiently few subbands popu-

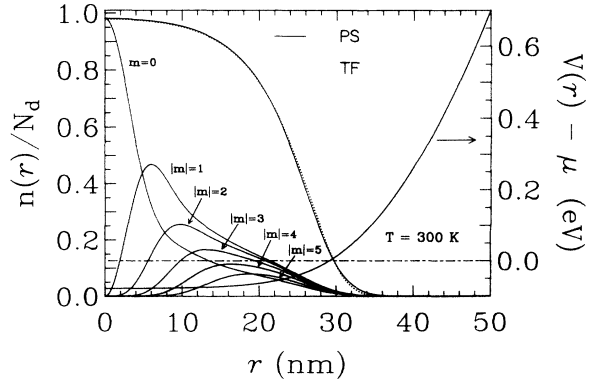

FIG. 5. Analogous to Fig. 3, except $T=300$ K. In this case, there are no discernible spatial oscillations in the electron density function. $N_d = 2\times10^{18}$ cm^{-3}.

lated that we expect Friedel-like oscillations to become apparent, and hence the greatest discrepancy between the PS and TF theories. For $T=300$ K, however, there are enough states that contribute to the electron density function that such oscillations are not apparent. In Fig. 5 we show the behavior of $n(r)$ and $V(r)$ for $T=300$ K, analogous to Fig. 3 (which applies to $T=10$ K). It is seen in Fig. 5 that there are no discernible Friedel oscillations and that the TF electron density function agrees well with that of the PS calculation. In general, we expect the PS results to go over to those of the corresponding TF theory whenever there are sufficiently many states that contribute to the summation in (6), such that the energy separation between successive eigenvalues is small compared to the thermal energy, $k_B T$.

IV. SUMMARY

In this paper, we have computed the self-consistent electron states and confining potential for cylindrical quantum wires with a Fermi-level-pinning boundary condition from a numerical solution of the coupled Poisson and Schrödinger equations. Finite-temperature effects have been included in the determination of the electron density function, which was derived from the one-electron density matrix in the grand-canonical ensemble using the self-consistent bound states. We have compared these results with those obtained from a finite-temperature Thomas-Fermi approximation. We find that in most cases, the TF results agree well with those of the more realistic, but also more computationally intensive, PS theory. At low temperatures or for cases where the structure is almost, but not completely depleted, the number of quantum-wire subbands that are populated is small, and both the electron density function and the confining potential exhibit Friedel-like spatial oscillations. Otherwise, when more than several subbands are populated, the TF theory, which is based on free-particle states, is remarkably accurate. We have also computed the partial electron density functions associated with any given value of the angular momentum quantum number. We find that the nonzero angular momentum states are relatively well populated in the interior of the cylindrical quantum wire.

We have shown that the form of the self-consistent potential is the result of a nonlinear screening process in which the electron density function, through the eigenstates of the system, depends sensitively upon such parameters as the temperature, the lateral dimension, material parameters, the doping density, and the boundary conditions. Besides being of scientific interest for the physics of confined electrons, nanostructures may also provide the basis for a revolutionary class of electron devices.[4,5] The properties of interest of such structures, e.g., the optical or transport characteristics, are ultimately a function of the electron eigenstates. Realistic modeling of the electron potential, such as exemplified in this paper, therefore provides not only a framework for understanding the physics of nanometer-scale structures, it also constitutes a practical *tool* for validating and refining concepts used in the design of nanostructure devices.

ACKNOWLEDGMENTS

We are indebted to R. T. Bate, W. R. Frensley, and Lutz Micheel. This work was supported in part by WL Contract No. F33615-87-C-1539, Nanoelectronic Development. Ames Laboratory is operated for the U.S. Department of Energy by Iowa State University under Contract No. W-7405-Eng-82.

---

*Present address: Department of Physics and Astronomy, Iowa State University, Ames, IA 50011.

[1]See, for example, *Nanostructures and Mesoscopic Systems,* edited by W. P. Kirk and M. A. Reed (Academic, New York, 1992); *Science and Engineering of One- and Zero-Dimensional Semiconductors,* edited by S. P. Beaumont and C. M. Sotomayor Torres (Plenum, New York, 1990).

[2]B. P. van der Gaag and A. Scherer, Appl. Phys. Lett. **56**, 481 (1990).

[3]J. N. Randall, M. A. Reed, J. H. Luscombe, G. A. Frazier, W. R. Frensley, A. C. Seabaugh, Y. C. Kao, T. M. Moore, and R. J. Matyi, Proc. SPIE **1284**, 66 (1990).

[4]R. T. Bate, Nanotechnology **1**, 1 (1990); G. A. Frazier, in *Concurrent Computations,* edited by S. K. Tewsburg, B. W. Dickinson, and S. C. Schwartz (Plenum, New York, 1988), p. 3; J. N. Randall, J. H. Luscombe, and R. T. Bate, in *Heterostructure and Quantum Devices,* edited by W. R. Frensley and N. G. Einspruch (Academic, New York, 1992).

[5]J. H. Luscombe, J. N. Randall, and A. M. Bouchard, Proc. IEEE **79**, 1117 (1991).

[6]See, for example, T. J. Thornton, M. Pepper, H. Ahmed, D. Andrews, and G. J. Davies, Phys. Rev. Lett. **56**, 1198 (1986); H. van Houten, B. J. van Wees, M. G. J. Heijman, and J. P. Andre, Appl. Phys. Lett. **49**, 1781 (1986); G. Timp, A. M. Chang, P. Mankiewich, R. Behringer, J. E. Cunningham, T. Y. Chang, and R. E. Howard, Phys. Rev. Lett. **59**, 732 (1987).

[7]M. A. Reed, J. N. Randall, R. J. Aggarwal, R. J. Matyi, T. M. Moore, and A. E. Wetsel, Phys. Rev. Lett. **60**, 535 (1988); J. N. Randall, M. A. Reed, T. M. Moore, R. J. Matyi, and J. W. Lee, J. Vac. Sci. Technol. B **6**, 302 (1988); M. A. Reed, J. N. Randall, and J. H. Luscombe, in *Localization and Confinement of Electrons in Semiconductors,* edited by F. Kuchar, A. Heinrich, and G. Bauer (Springer, New York, 1990), p. 20.

[8]T. P. Smith III, K. Y. Lee, C. M. Knoedler, J. M. Hong, and D. P. Kern, Phys. Rev. B **38**, 2172 (1988); S. Tarucha, Y. Hirayama, T. Saku, and T. Kimura, *ibid.* **41**, 5459 (1990); A. Lorke, J. P. Kotthaus, and K. Ploog, Phys. Rev. Lett. **64**, 2559 (1990), and references therein.

[9]J. H. Luscombe and M. Luban, Appl. Phys. Lett. **57**, 61 (1990).

[10]See, for example, J. S. Blakemore, Solid State Electron. **25**, 1067 (1982), for a review of the properties of Fermi-Dirac integrals.

[11]J. H. Luscombe and W. R. Frensley, Nanotechnology **1**, 131 (1990); J. H. Luscombe, in *Nanostructures and Mesoscopic Systems* (Ref. 1), p. 357; A. M. Bouchard, J. H. Luscombe, A.

C. Seabaugh, and J. N. Randall, *ibid.*, p. 393.

[12]A. Zangwill, *Physics at Surfaces* (Cambridge University Press, New York, 1988), p. 96. Fermi-level pinning is accomplished through the occupation of unfilled states at the surface, which have a much greater areal density than do bulk states near the surface.

[13]M. A. Reed, J. N. Randall, J. H. Luscombe, W. R. Frensley, R. J. Aggarwal, R. J. Matyi, T. M. Moore, and A. E. Wetsel, in *Advances in Solid State Physics,* edited by U. Rossler (Vieweg, Braunschweig, 1989), Vol. 29, p. 267.

[14]M. Luban, J. H. Luscombe, M. A. Reed, and D. Pursey, Appl. Phys. Lett. **54**, 1997 (1989). This theoretical conclusion must now be partially discounted in that it ignored the effects of lateral quantization in the quantum-wire contacts to the quantum-dot nanostructure. See G. W. Bryant, Phys. Rev. B **44**, 3064 (1991), where such effects are taken into account. It is now clear that a full tunneling theory of the complete nanostructure system (quantum dot plus quantum wire) is required to elucidate the role of the nonzero angular momentum states in contributing to the tunneling current.

[15]This boundary condition is a consequence of the exposed lateral surface, where the electron affinity to the vacuum presents a large potential barrier for penetration of the wave function outside the system. The boundary condition would be modified, of course, for systems where lateral confinement is achieved by some other means, e.g., by lateral heterojunctions. See Ref. 5.

[16]H. J. Kreuzer, *Nonequilibrium Thermodynamics and its Statistical Foundations* (Oxford, New York, 1981), p. 212.

[17]J. H. Wilkinson, *The Algebraic Eigenvalue Problem* (Oxford, New York, 1965), Sec. 66.

[18]See, for example, B. T. Smith *et al.*, *Matrix Eigensystem Routines–EISPACK Guide,* 2nd ed., Lecture Notes in Computer Science Vol. 6 (Springer, New York, 1976).

[19]S. E. Laux and A. C. Warren, *IEDM, Technical Digest 1986* (IEEE, New York, 1986), p. 567; S. E. Laux, in *Proceedings of Numerical Analysis of Semiconductor Devices and Integrated Circuits V* (Boule, Dun Laoghaire, Ireland, 1987), p. 270; S. E. Laux and F. Stern, Appl. Phys. Lett. **49**, 91 (1986). See also S. Selberherr, *Analysis and Simulation of Semiconductor Devices* (Springer-Verlag, New York, 1984), p. 206.

[20]R. E. Bank and D. J. Rose, SIAM J. Numer. Anal. **17**, 806 (1980).

[21]J. M. Ziman, *Principles of the Theory of Solids* (Cambridge University Press, Cambridge, 1972), p. 157.

[22]We note that for this doping density the confining potentials are nominally identical for the two temperatures, and the differences in eigenvalues for the two temperatures are not discernible on the scale of Fig. 4. The set of eigenvalues for $T = 300$ K is shown.